A Layman's

Interpretation Guide

to

L-band and C-band

Synthetic Aperture Radar data

Version 3.0 (May 2023)

Table of Contents

1   About this guide

This "layman's" guide was developed to provide users who have little or no experience of spaceborne Synthetic Aperture Radar (SAR) data with a simple reference document that outlines some basic concepts of radar remote sensing, presents some commonly used SAR datasets, and provides some examples of how a few different land cover types may appear in SAR imagery.

The guide does not go into the depths of microwave theory or radar processing (there is plenty of literature covering that) as expert knowledge today no longer should need to be a major concern for most users. Many space data providers are also now moving towards the provision of so called analysis-ready data also for SAR, which can be used and integrated with other data sources with little or no need for users to undertake their own processing.

That said, some basic understanding of SAR technology and how radar signals interact with the ground is nevertheless required to properly utilise SAR data, as the concept of radar and microwaves is different from that of traditional optics. Different, but not necessarily difficult.

2   Briefly about Synthetic Aperture Radar

2.1   The radar wavelength

Synthetic Aperture Radar, SAR, is an active system operating in the microwave domain of the electromagnetic spectrum. Microwaves are not visible to the human eye and provide a very different view of the world from what we are used to.

While optical remote sensing sensors function similar to the human eye – they are passive sensors which record reflected sunlight – a radar sensor operates more like a flash camera in a dark room. The radar emits a light pulse and records the part of the pulse that is reflected, or scattered, back to the sensor (hence the term backscatter). Unlike sunlight which is non-polarised and comprises a large range of different wavelengths, the radar is a laser which operates within narrow and well-defined wavelength bands, and at a specific polarisation.

Common present and near-future spaceborne radar systems operate with the following bands:

- P-band: ~69.0 cm (BIOMASS)
- L-band: ~23.5 cm (ALOS -2 PALSAR-2, ALOS-4 PALSAR-3, SAOCOM-1, NISAR-L)
- S-band: ~9.4 cm (NovaSAR, NISAR-S)
- C-band: ~5.6 cm (Sentinel-1, Radarsat-2, RCM)
- X-band: ~3.1 cm (TerraSAR-X, TanDEM-X, COSMO-SkyMed, RISAT)

The choice of wavelength band strongly affects what type (size) of objects the radar is sensitive to. As a rule of thumb, the radar "can see" objects of about the same spatial magnitude as the radar wavelength, and larger. Objects significantly smaller than the radar wavelength, become transparent to the radar, although they cause certain attenuation of the signal. The smaller the objects, the less influence (attenuation) on the backscatter.

Longer wavelength radar signals (such as L-band) consequently penetrate through the forest canopy (since the small leaves are transparent) and interact with the larger structures such as the trunks and larger branches of trees – and hence display a positive, although limited, correlation with above-ground biomass. Systems operating at shorter wavelengths (such as C-band) on the other hand, are more sensitive to sparse and low biomass vegetation.

2.2 Polarisation

The radar polarisation is another parameter affecting the strength of the backscatter. Current spaceborne radar systems operate with linear polarisation, where the radar signals are transmitted and received at horizontal (H) and/or vertical (V) polarisation.

The polarisation of SAR imagery are commonly denoted by two letters, the first indicating the transmitted polarisation and the latter the received polarisation.

- HH: Transmission of horizontal wave; Reception of horizontal component
- HV: Horizontal transmission; Vertical reception
- VH: Vertical transmission; Horizontal reception
- VV: Vertical transmission; Vertical reception
- Quad-pol (QP): H and V transmission; H and V reception (HH+HV+VH+VV)

HH and VV are commonly referred to as co-polarisation (or like-polarisation) backscatter components, while cross-polarisation connotes HV and VH.

2.3 Radar backscatter

2.3.1 Sigma-nought

Radar image brightness is normally expressed in σ^o (*sigma-nought*) which is the radar backscatter per unit area. The unit of σ^o is [m2/m2], expressed in decibel (dB).

The standard formula to calculate σ^o from <u>backscatter amplitude</u> is:

$\sigma^o = 10 * \log_{10}(\Sigma[DN^2]) + K$

where DN is the image pixel digital number measured in the SAR amplitude image. Due to speckle , and $\Sigma[DN^2]$ indicates the average squared DN value over a group of (homogeneous) pixels (or more accurately, the average pixel value over a group of pixels).

In case the data are provided as <u>backscatter power</u> (where $DN_{power} = [DN_{amplitude}]^2$) the formula becomes:

$\sigma^o = 10 * \log_{10}(DN) + K$

K is a calibration factor which varies depending on the SAR sensor and processor system used.

2.3.2 Gamma-nought

Even for homogeneous targets, σ^o varies depending on the angle between the ground normal and the sensor – the local incidence angle – being higher (brighter) in the near-range part of the image (closest to the satellite) and lower (darker) in the far-range of the image, further away from the satellite. By normalising σ^o with respect to the incidence angle we can remove some (but not all) of the range-dependency to obtain γ^o (*gamma-nought*):

$\gamma^o = \sigma^o/\cos\varphi$,   where φ is the local incidence angle.
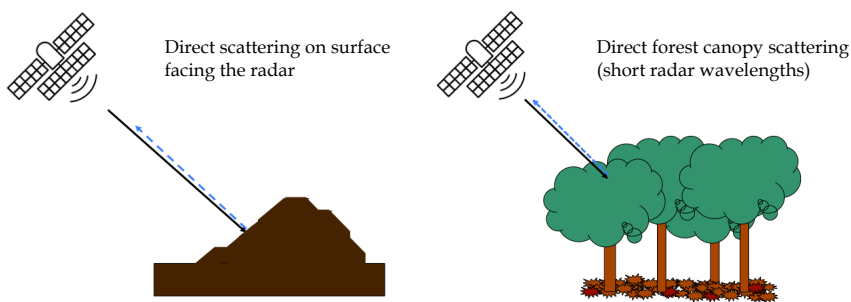
2.4 Backscatter mechanisms

In order to accurately interpret the content of a SAR image, some basic understanding of how radar signals interact with different land cover types is required. Below follows a short description of some of the most important backscatter mechanisms to keep in mind.
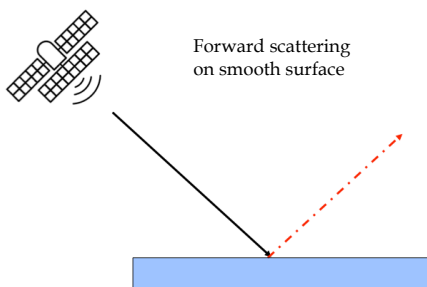
2.4.1 Direct backscatter

Direct backscatter occurs when the transmitted signal is reflected directly back to the sensor by a single reflection, by a surface oriented perpendicular to the radar illumination direction. It results in a strong co-polarisation (HH or VV) reflection and appears bright in the SAR image.

Rock outcrops or bare mountain slopes oriented towards the radar can produce direct backscattering. At the short C-band wavelength, also the leaves in a dense vegetation canopy can cause direct scattering.

Direct scattering on surface facing the radar

Direct forest canopy scattering (short radar wavelengths)

2.4.2 Forward scattering

A smooth surface (relative to the radar wavelength), such as a calm water surface or (at longer wavelengths) a bare soil area results in little or no scattering back towards the radar antenna as the transmitted signal reflects once on the surface and continues its path away from the SAR antenna. Areas with forward scattering appear dark in the SAR image in both co- and cross-polarisation.

Forward scattering on smooth surface

2.4.3 Diffuse scattering
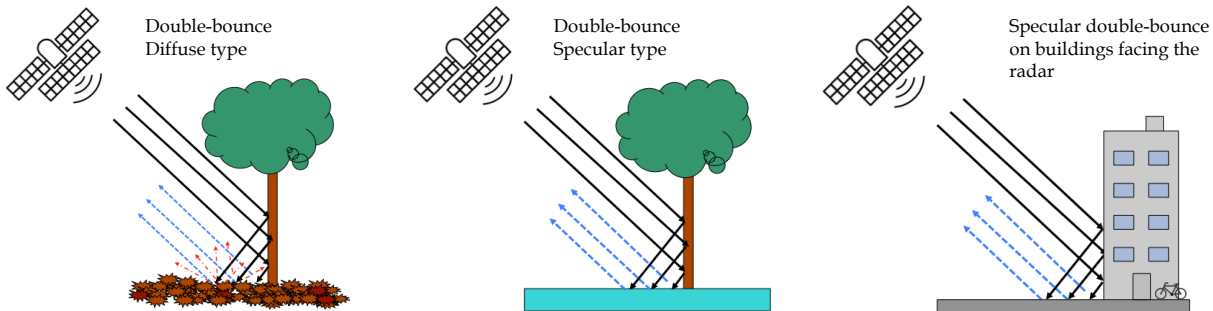
A rough surface (relative to the radar wavelength), such as a ploughed field or waves on water, results in the signal being scattered in different directions. The component reflected back towards the radar (direct scatter) is measured. The rougher the surface, the higher the (co-pol) backscatter.

Diffuse scattering on "rough" surface

Diffuse scattering on rough water surface

2.4.4a Double-bounce scattering

When the targets and ground surface are perpendicular, such as vertical tree stems on flat ground, they can act as corner reflectors, providing a "double-bounce" scattering effect that sends the radar signals back in the same direction they came from. Since multiple radar waves reflecting on a particular vertical target travel the exactly same total distance, no matter where on the target the reflection occurs, all returning waves remain coherent (have the same phase) and thus result in a strongly enhanced return signal. As reflections on vertical targets do not alter the polarisation direction of the radar signals, double-bounce scattering occurs only at co-polarisation.

Double-bounce Diffuse type

Double-bounce Specular type

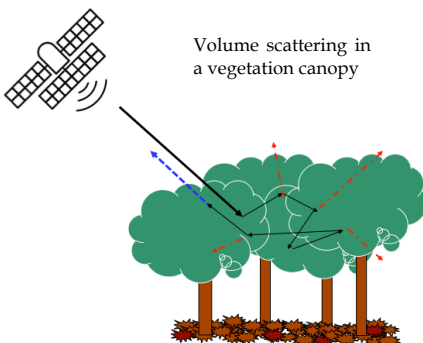Specular double-bounce on buildings facing the radar

2.4.4b Double-bounce scattering – specular type

In the case the forest floor is flooded, the diffuse scatter on the ground is replaced with a (loss-less) specular reflection on the water surface, resulting in a particularly strong co-polarised return signal. Specular double-bounce scattering can under certain circumstances also be observed e.g. in urban areas with buildings oriented towards the radar, in open waters by ships, bridges and oil platforms, as well as in irrigated rice fields through interactions between the plant stems (when vertical) and the water surface.

2.4.5 Volume scattering

Volume scattering occurs when the radar signal is subject to multiple reflections within 3-dimensional matter. At L-band, a common type of volume scattering is the one that occurs on twigs and branches within a forest canopy. At the shorter C-band wavelength, volume scattering can take place within the canopies of lower or sparse vegetation types, such as bushes, shrubs or agricultural crops. Since the orientations of the main scatterers are random, the polarisation of the backscattered signal is also random, rendering equal backscatter in co- and cross-polarisation.

Volume scattering in a vegetation canopy

It should be noted that the scattering mechanisms described above seldom occur in isolation. The backscatter for a particular land cover type observed in a SAR image is typically the result of a combination of several mechanisms, where the total backscatter measured is the sum of the relevant different contributions ($\gamma^o_{TOTAL} = \gamma^o_{DIRECT} + \gamma^o_{DOUBLE-BOUNCE} + \gamma^o_{VOLUME} + \gamma^o_{ETC}$)

3 Synthetic Aperture Radar data used in this guide

3.1 L-band SAR data

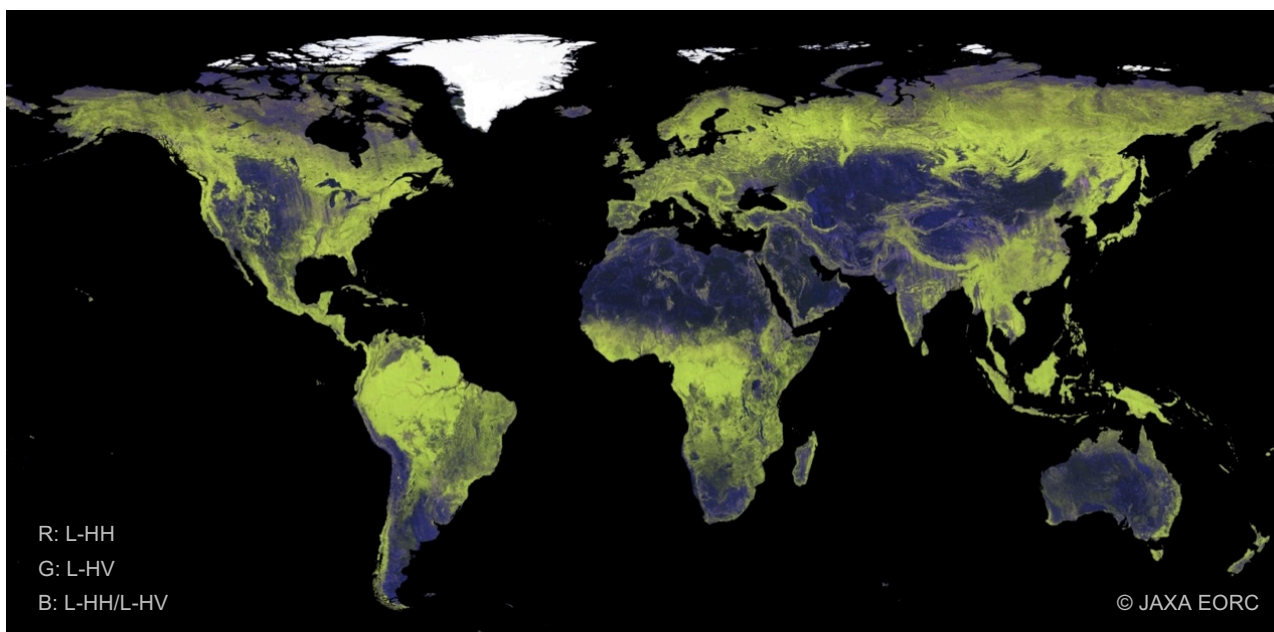### 3.1.1 ALOS PALSAR mission series

The Advanced Land Observing Satellite 2 (ALOS-2) was launched by the Japan Aerospace Exploration Agency (JAXA) in 2014. It carries a Synthetic Aperture Radar (PALSAR-2) instrument which operates in L-band (23.5 cm) wavelength. It provides single, dual and full polarisation capability and observation modes with varying ground resolutions (1 m ~ 100 m) and imaging swath widths (25 km ~ 500 km). ALOS-2 operates with a 14-day (ground track) repeat cycle.

The ALOS-2 mission was preceded by ALOS PALSAR (2006-2011) and JERS-1 SAR (1992-1998). All three missions have been subject to global systematic observation strategies and a consistent archive of L-band SAR data dating back to the mid-1990s therefore exists for most areas in the world, with higher density in the tropics. ALOS-2 will be succeeded by ALOS-4 PALSAR-3, that is scheduled for launch in 2024.

3.1.2 ALOS-2 PALSAR-2 global mosaics

For this user guide, 25 m pixel spacing global mosaic data generated from ALOS-2 PALSAR-2 dual polarisation (HH + HV) data acquired in 10 m ground resolution stripmap mode were used. The mosaics were generated by assembling adjacent satellite observation swaths, each 70 km wide and up to several thousand km long, to form a seamless global mosaic. The original 10 m resolution data were resampled (averaged) to 25 m (0.8 arcsec) pixel spacing. The (global) incidence angles vary between 28.5° (near range, closest to the satellite) and 42.5° (far range).

To avoid huge data files, the mosaics are provided in tiles, 1° by 1° in latitude and longitude direction.

ALOS PALSAR global mosaic at 25 m (0.8 arcsec) pixel spacing.
HH+HV polarisation composite (R:HH; G:HV; B:HH/HV).

6

JAXA generates global mosaics on an annual basis. ALOS-2 PALSAR-2 mosaics are currently available for the years 2015–2022; ALOS PALSAR mosaics for 2007–2010; and one JERS-1 SAR global mosaic assembled from data acquired between 1995 and 1997. All global mosaic data can be downloaded free of charge at: https://www.eorc.jaxa.jp/ALOS/en/palsar_fnf/fnf_index.htm

The JAXA global mosaic datasets are compliant with *CEOS Analysis Ready Data (ARD)*, Normalised Radar Backscatter (NRB v5.5) standards, meaning that they have been have been subject to full geometric and radiometric corrections and organised into a form, and with corresponding metadata, that should allow immediate analysis with a minimum of additional user effort.

3.1.2.1 Geometric and radiometric corrections

The mosaics are ortho-rectified using the ALOS PRISM AW3D30 30 m (1 arcsec) Digital Elevation Model. The mosaics are provided in geographical (lat/long) coordinates (EPSG 4326), using the WGS84 datum and ellipsoid. The original 10 m stripmap data have been resampled (averaged) to pixel spacing of 0.8 arc seconds, corresponding to approximately 24.7 m at the Equator[1].

Full Radiometric Terrain Correction (RTC) using the AW3D30 DEM has been applied to correct for incidence angle and topographic effects on image intensity, giving the images a "flat" look as terrain relief effects have been removed. The backscatter is provided as gamma-nought (γ^o).

3.1.2.2 Image and metadata

The mosaic datasets comprise five separate images/layers:

- Radar backscatter (γ^o) – HH polarisation
- Radar backscatter (γ^o) – HV polarisation
- Local incidence angle
- Observation date image
- Mask image

File name convention: **AAABBBB_YY_[layer indicator],** where
    AAA: latitude of tile upper left corner [e.g. S01]
    BBBB: longitude of tile upper left corner [e.g. E041]
    YY: two last digits of mosaic year [e.g. 09 for 2009]
    [layer indicator]: "sl_HH"; "sl_HV"; "date"; "linci"; "mask"

ALOS-2 mosaics have the additional extension "_F02DAR", where
    F02: Stripmap Fine Beam, mode #2
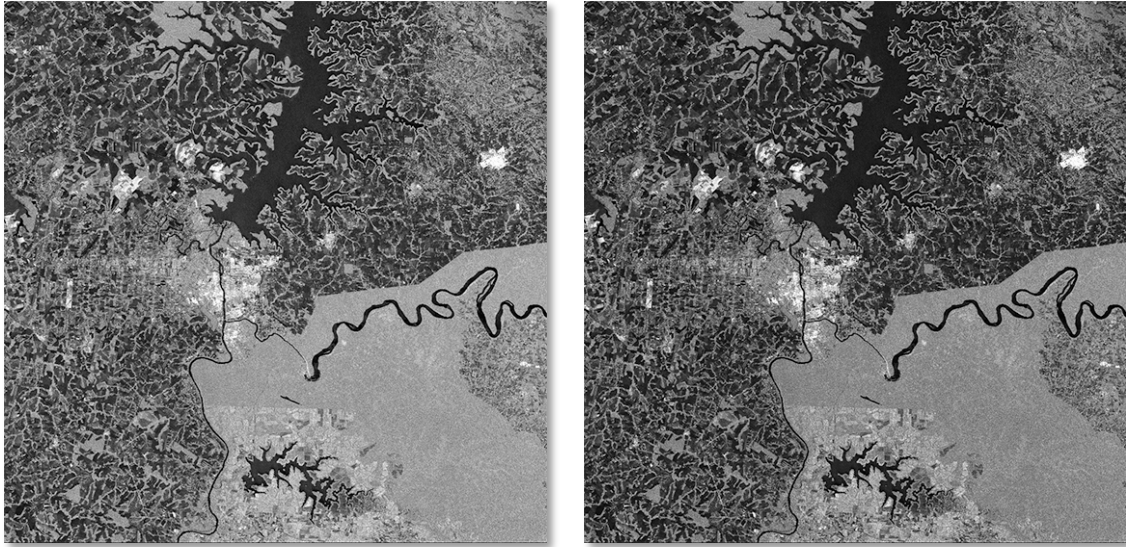   **D:** Dual polarisation
    A: Ascending pass
    R: Right-Looking

---

[1] Note that geographical coordinates result in a pixel spacing that varies in latitude direction, with the actual pixel area at latitude ϕ being 24.7 x 24.7 x cosϕ [m2]. The mosaics therefore need to be converted to an equal-area projection in case they are to be used for area measurements.

3.1.2.3   Data Layer description

Radar backscatter

Backscatter images – HH polarisation (left); HV polarisation (right)
(Paraná/Iguazu river confluence, Paraguay, Brazil, Argentina / mosaic tile S25°/W055°)

Content: Calibrated radar backscatter amplitude at HH polarisation and HV polarisation.

Data type: 16 bits Unsigned Integer (UINT16)

Format: Cloud optimized GeoTIFF (COG)

Dimensions: 4500 pixels x 4500 lines

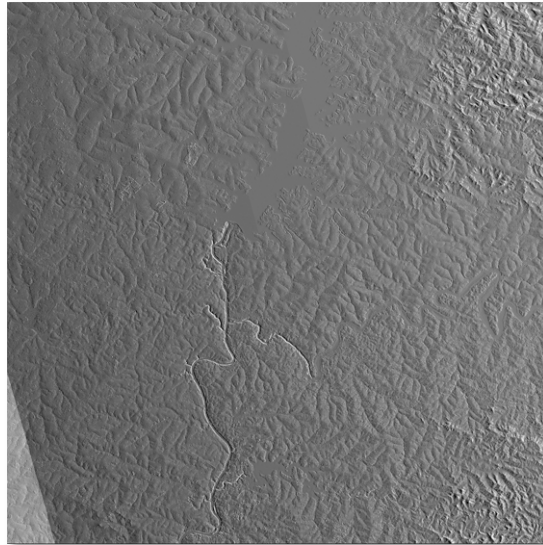**File names:** AAABBBB_YY_[**sl_HH**]

AAABBBB_YY_[**sl_HV**]

Radar backscatter amplitude is provided as two separate images: one for the Horizontal-Horizontal (HH) polarisation, and one for Horizontal-Vertical (HV) ditto. The backscatter images constitute the data files on which all analysis should be undertaken.

The linear amplitude backscatter values in the HH and HV images can be converted from image digital numbers (DN) to γ^o, and expressed in decibel (dB), by the equation:

$$\gamma^o = 10 * \log_{10}(\Sigma[DN^2]) - 83.0$$

where $\Sigma[DN^2]$ indicates the average squared DN value over a group of (homogeneous) pixels, and -83.0 dB is the calibration factor (K) used by JAXA.

Local incidence angle

Local incidence angle image

Content: Image showing the local incidence angle [unit: degrees]

Data type: 8 bits (BYTE)

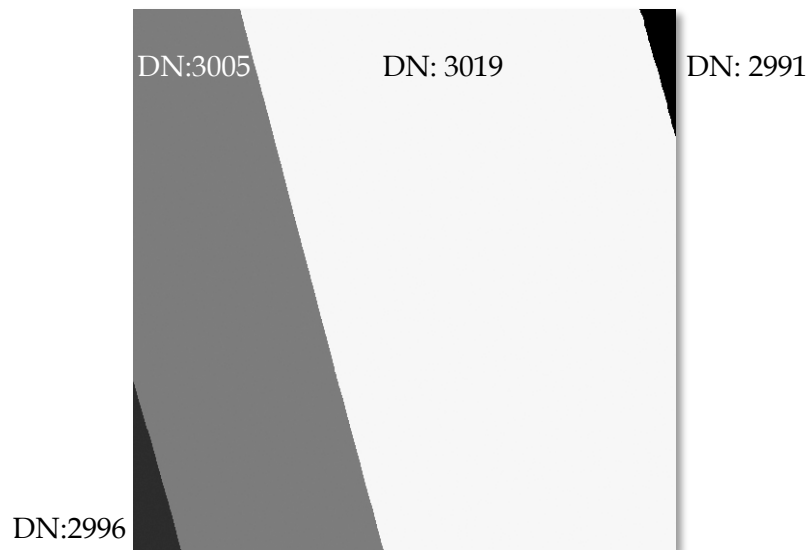**Format:** Cloud optimized GeoTIFF (COG)

Dimensions: 4500 pixels x 4500 lines

File name: AAABBBB_YY_[**linci**]

The incidence angle image is derived from the (ALOS PRISM) AW3D30 Digital Elevation Model used for geometric and radiometric correction. It has the same dimensions as the backscatter images and provides information about local incidence angle, i.e. the angle between Earth normal at the pixel location and the SAR sensor, for each pixel in the image.

The pixel value in the local incidence angle image indicates the angle in degrees. On flat ground, the incidence angles for ALOS-2 PALSAR-2 beams used for the global mosaics vary from about 28° in near range, to about 42° in far range.

Observation date image

Observation date image

DN:3005 DN: 3019 DN: 2991

DN:2996

Observation date image

Content: Image showing the observation date for each pixel

Data type: 16 bits Unsigned Integer (UINT16)

Format: Cloud optimized GeoTIFF (COG)

Dimensions: 4500 pixels x 4500 lines

File name: AAABBBB_YY_[**date**]

As the mosaic tiles are composed of SAR data from multiple satellite paths, an observation date image is required to provide information about the date of acquisition for each pixel in the mosaic tile.

The (16 bits) pixel digital numbers in the observation date image correspond to the number of days after the launches of ALOS-2 and ALOS and JERS-1 satellites, respectively. ALOS-2 was launched on May 24, 2014 (used for the 2015-2022 mosaics), ALOS on Jan. 24, 2006 (used for the 2007- 2010 mosaics), and JERS-1 on Feb. 11, 1992 (used for the 1996 mosaic).

The Digital Numbers in the ALOS-2 mosaic observation date image above thus correspond to:
24/05/2014 + 2991 = 01/08/2022
24/05/2014 + 2996 = 06/08/2022
24/05/2014 + 3005 = 15/08/2022
24/05/2014 + 3019 = 29/08/2022

Note that dates are provided in UTC (Coordinated Universal Time), which, depending on the geographic location, may differ from the local date the observation took place.

10

Mask image

Value	Category
0	No data
50	Ocean water
100	Layover
150	Shadowing
255	Land

Mask image and Look-up table of DN values

Content: Mask image

Data type: 8 bits (BYTE)

Format: Cloud optimized GeoTIFF (COG)

Dimensions: 4500 pixels x 4500 lines

File name: AAABBBB_YY_[**mask**]

The mask image indicates pixels affected by radar-specific geometric distortions; including *layover* (causing tall objects to be displaced towards the sensor) [DN=100] and *radar shadowing* (areas not illuminated by the radar, such as e.g. the backside of steep mountains) [DN=150].

The mask image also contains information about no-data [DN=0] and ocean water pixels [DN=50].

Valid land pixels, including inland water bodies and rivers, are assigned DN value 255.

General metadata

```xml
<?xml version="1.0" encoding="utf-8"?>
<Product type="Normalised Radar Backscatter" version="5.5" copyright="JAXA/EORC">
    <DocumentIdentifier type="URL">https://ceos.org/ard/files/PFS/NRB/v5.5/CARD4L-PFS_NRB_v5.5.pdf</DocumentIdentifier>
    <DataCollectionTime>
        <NumberOfAcquisitions>4</NumberOfAcquisitions>
        <FirstAcquisitionDate>2022-08-01</FirstAcquisitionDate>
        <LastAcquisitionDate>2022-08-29</LastAcquisitionDate>
    </DataCollectionTime>
    <SourceAttributes acqID="1">
        <SourceDataRepository type="URL">https://gportal.jaxa.jp/gpr/?lang=en</SourceDataRepository>
        <Satellite>ALOS-2</Satellite>
        <Instrument>PALSAR-2</Instrument>
        <SatelliteReference type="URL">https://directory.eoportal.org/web/eoportal/satellite-missions/a/alos-2</SatelliteReference>
        <SourceDataAcquisitionTime>
            <StartTime>2022-08-06T04:14:24.792Z</StartTime>
            <EndTime>2022-08-06T04:16:02.947Z</EndTime>
        </SourceDataAcquisitionTime>
        <SourceDataAcquisitionParameters>
            <RadarBand>L</RadarBand>
            <RadarCenterFrequency units="Hz">1.2365e+09</RadarCenterFrequency>
            <ObservationMode>Stripmap FBD</ObservationMode>
            <RadarBandWidth units="Hz">2.8e+07</RadarBandWidth>
            <Polarizations>HH+HV</Polarizations>
            <AntennaPointing>Right</AntennaPointing>
            <BeamID>F2-7</BeamID>
            <RSP_PathNumber>24</RSP_PathNumber>
        </SourceDataAcquisitionParameters>
        <OrbitInformation>
            <PassDirection>Ascending</PassDirection>
            <OrbitDataSource>Precise</OrbitDataSource>
        </OrbitInformation>
        <SourceProcParam>
            <ProcessingFacility>JAXA/EORC</ProcessingFacility>
            <ProcessingDate>2023-03-28T01:45:08.052Z</ProcessingDate>
```

Extract from XML metadata file (example)

Content: General metadata

Format: XML

File name: AAABBBB_YY_[xxx]**.xml**

Each mosaic tile is accompanied by a general metadata file which contains comprehensive information about the mosaic product, including e.g. the source data used, radiometric and geometric corrections applied, and ancillary datasets. It is formatted in accordance with CEOS Analysis Ready Data XML specifications.
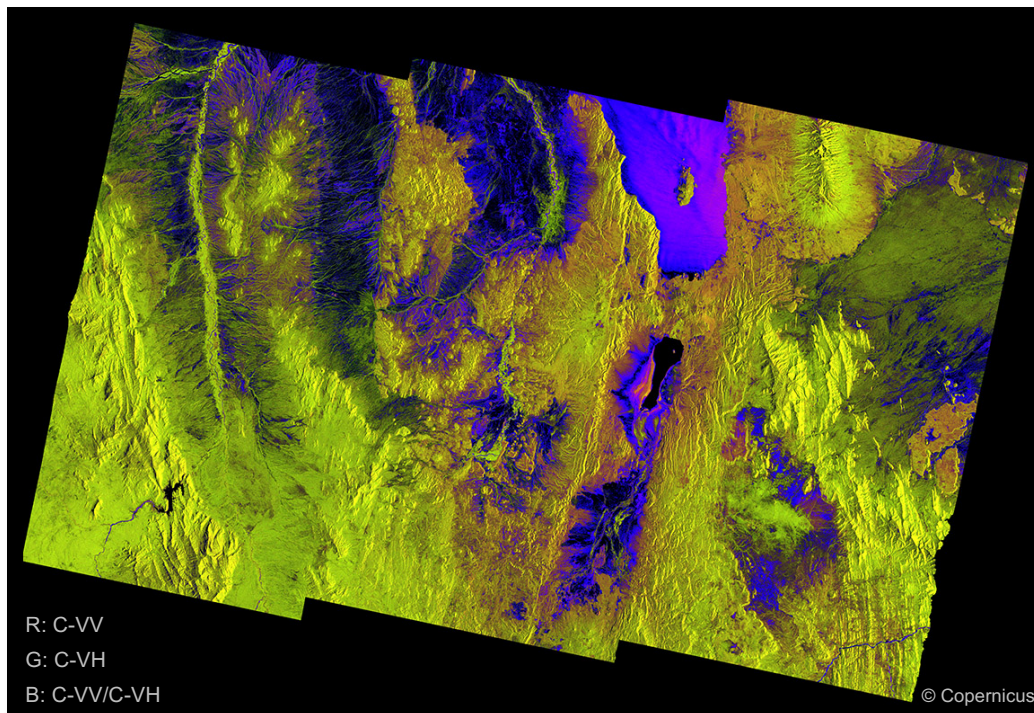
Full mosaic dataset description from JAXA is available at:
https://www.eorc.jaxa.jp/ALOS/en/dataset/pdf/DatasetDescription_PALSAR2_Mosaic_ver212.pdf

3.2 C-band SAR data

3.2.1 Copernicus Sentinel-1

The Sentinel-1 mission constitutes the radar component of the Copernicus joint initiative of the European Commission (EC) and the European Space Agency (ESA). The Sentinel-1 mission is composed of a constellation of two satellites, which provides 12-day (ground track) repeat cycle for one satellite, and 6-day (ground track) repeat for two satellites[2]. Taking advantage of converging satellite tracks at higher latitudes and the possibility to observe in both ascending (south-to-north) and descending (north-to-south) directions, a given ground location can be covered at even higher frequency (such as the case is for Europe).

Sentinel-1 operates in C-band (5.6 cm) wavelength and provides single or dual polarisation capability. For this guide, VV and VH dual polarisation data acquired in Interferometric Wide (IW) swath mode have been used. The IW mode images the ground with three sub-swaths (see figure below) which provide a combined 250 km swath width with an incidence angle variation across the swath between 29.1° (near range) and 46.0° (far range). The "raw" spatial resolution of the sensor in IW mode is about 3 m in range direction (perpendicular to the satellite velocity vector) and 22 m in azimuth (parallel to the satellite track). The pixel spacing of the user products vary depending on product type and processing level (see 3.2.2. below).

R: C-VV
G: C-VH
B: C-VV/C-VH
© Copernicus

Sentinel-1 Interferometric Wide (IW) Swath. VV+VH polarisation composite
(Turkana/Samburu, Kenya, 6-OCT-2017)

---

[2] Since December 2021, only Sentinel-1A is operational following a failure of Sentinel-1B. The constellation is scheduled to be replenished by Sentinel-1C in 2023.

Free and open-access Sentinel-1 SAR data are available through the Copernicus Open Access Hub (https://scihub.copernicus.eu) and the Alaska Satellite Facility (https://www.asf.alaska.edu/sentinel).

3.2.2 SNAP and data formats

Two SAR processors were used to generated the Sentinel-1 imagery shown in this Guide – the SentinelHub CARD4L Tool (https://apps.sentinel-hub.com/s1-card4l/) and the Sentinel Application Platform (SNAP). SNAP is a collection of executable tools and Application Programming Interfaces (APIs) which have been developed to facilitate the utilisation, viewing, and processing of a variety of satellite data. SNAP is a free software developed and distributed under the terms of GNU General Public License and comes with full Java source code available on GitHub. The SNAP toolbox can ingest either Single-Look Complex (SLC) or Ground Range Detected (GRD) product level data.

Single-Look Complex (SLC) products are images in the slant range, geo-referenced using orbit and attitude data from the satellite. As the name indicates, SLC products are single-look, meaning that they have not been averaged (multi-looked) and hence comprise full speckle information. In slant range geometry, the pixel spacing in range and azimuth are different (2.3m and 14.1m respectively for ESA products). Each image pixel is represented by a complex (I and Q) number and thus contains both amplitude and phase information. SLC level data are required for interferometric or polarimetric (e.g. polarimetric decomposition) applications.

Ground Range Detected (GRD) level data contain no phase information. For applications where only backscatter is of interest, GRD data, which are significantly smaller in size than SLC, would be recommended. GRD products have been multi-looked (averaged) and projected from slant range (sensor look direction) to ground range onto an Earth ellipsoid model. High Resolution (HR) IW GRD products from ESA have approximately square spatial resolution (20m x 22m) with reduced speckle due to the multi-look processing. To ease utilisation GRD products are resampled to square pixel spacing, with 10m x 10m or 20m x 20m commonly used. For more details about Sentinel-1 products, please refer to the ESA Technical Guides.

3.2.3 Geometric and radiometric corrections

The Sentinel-1 dual polarisation (VV+VH) High Resolution IW mode data used in this guide were geometrically corrected using 30 m Digital Elevation Model (Copernicus DEM by the SentinelHub) and SRTM by SNAP) and projected to the same geographical lat/long grid as the PALSAR-2 mosaics. The data were corrected for near-far range incidence angle variations and are thus given as gamma-nought (γ^o). Radiometric slope corrections (Radiometric Terrain Correction, RTC) were undertaken by the SentinelHub but was not available by SNAP and terrain relief effects therefore remain in the SNAP images, as can be seen in some of of the examples in section 3 below.

The SNAP output data, given in 32 bits FLOAT format, represent backscatter *power,* and the VV and VH images were thus converted from image digital numbers (DN) to γ^o by the equation:

$$\gamma^o = 10 * \log_{10}(<DN>) \text{ [dB]}$$

where <DN> indicates the the averaged power pixel value over a group of pixels.

4   Simple SAR interpretation guide

4.1   Cautions when using this guide

Below follow a number of examples of how some different land cover types around the globe can appear in (ALOS-2 PALSAR-2) HH and HV polarisation L-band SAR and (Sentinel-1) VV and VH polarisation C-band SAR data. In an effort to minimise backscatter variations due to temporal differences between the L- and C-band data, PALSAR-2 and Sentinel-1 data acquired as close in time as possible were selected. Time differences vary between a few days (in most cases) to several months (in a few cases). The observation dates are indicated.

It should be noted that the backscatter values given below the images represent the values measured in that particular image, given its local vegetation characteristics and local weather and seasonal conditions at the time of acquisition. So while the values are indeed meant to provide a feeling of typical responses for different land cover types, they should be considered indications only. To provide a hint of the backscatter variability, the standard deviations measured are also given (in brackets).
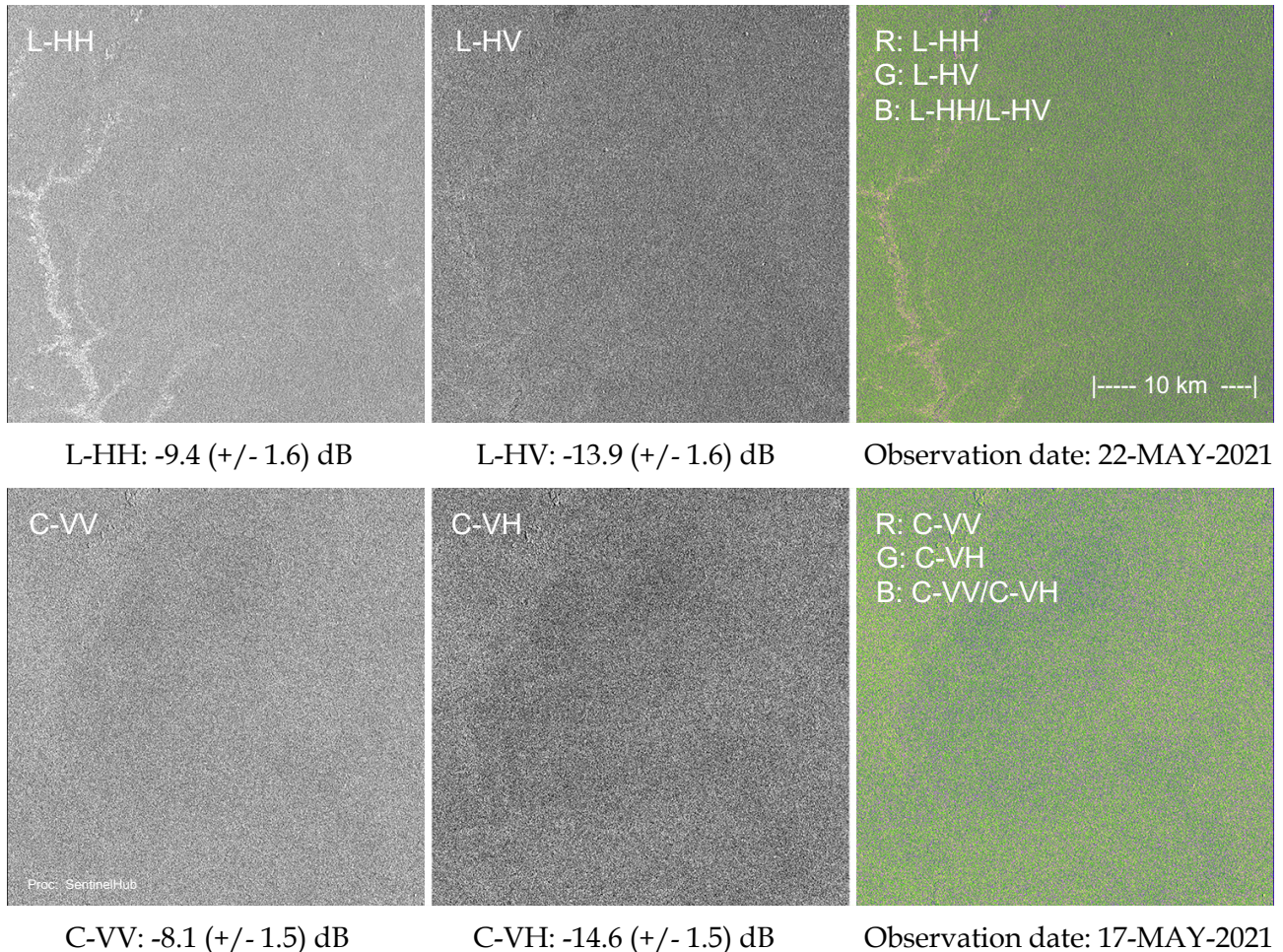
The backscatter images in the figures have been scaled from the original 16 and 32 bits data for visualisation purposes. While for instance the cross-polarisation (HV and VH) backscatter typically is lower (darker) than that of the co-polarisation channels (HH and VV), the two channels can look similar in the examples as different scaling factors have been used to maximise the visual impression.

RGB colour composite images are shown for reference, although it is important to keep in mind that there are neither any standardised rules on how represent microwave data visually, nor how to compose a 3-channel colour image from only two input channels. Yet, the [HH, HV, HH/HV] and [VV, VH, VV/VH] combinations used here for [R, G, B] for PALSAR-2 and Sentinel-1 respectively, are frequently utilised by remote sensing users.

Finally it should be noted that the examples in this guide all show single-date images, which, as mentioned above, are susceptive to the local physical ground and atmospheric conditions which may vary considerably over time. For analysis of SAR data, multi-temporal time-series data are therefore commonly used both to reduce temporal "noise" in the data, as well as to better characterise highly dynamic land cover and land use types such as e.g. agriculture and wetland inundation.

4.2 Examples

4.2.1 Dense tropical forest (Colombia)

| L-HH: -9.4 (+/- 1.6) dB | L-HV: -13.9 (+/- 1.6) dB | Observation date: 22-MAY-2021 |
| C-VV: -8.1 (+/- 1.5) dB | C-VH: -14.6 (+/- 1.5) dB | Observation date: 17-MAY-2021 |

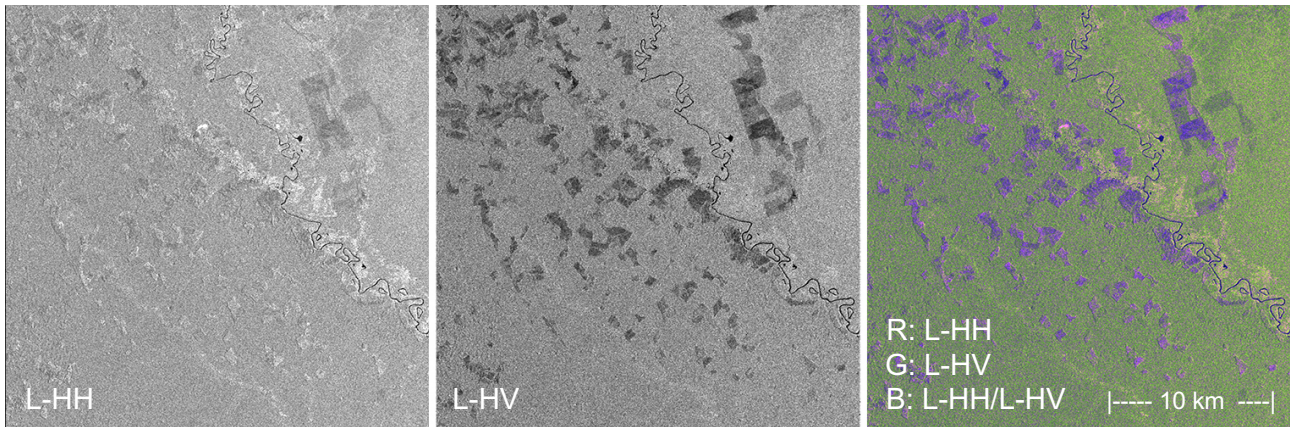Location: Caqueta, Colombia (N0.35°, W74.30°). Dense tropical rain forest in flat terrain.

L-band:

Dense homogeneous forest results in high and uniform L-band backscatter at both HH and HV polarisations. The long wavelength (23.5 cm) L-band signal penetrates through the forest canopy (leaves typically being smaller than the radar wavelength) and interacts with twigs, branches and stems. The L-band backscatter is therefore closely correlated with forest structure.

C-band:

At the shorter (5.6 cm) C-band wavelength, dense tropical forests display uniform backscatter in both the VV and VH channels. At VV polarisation, strong direct backscatter on the leaves constitute the dominating backscatter mechanism. Penetration through a closed canopy is limited at C-band, and therefore also volume scattering, resulting in low backscatter at VH polarisation.
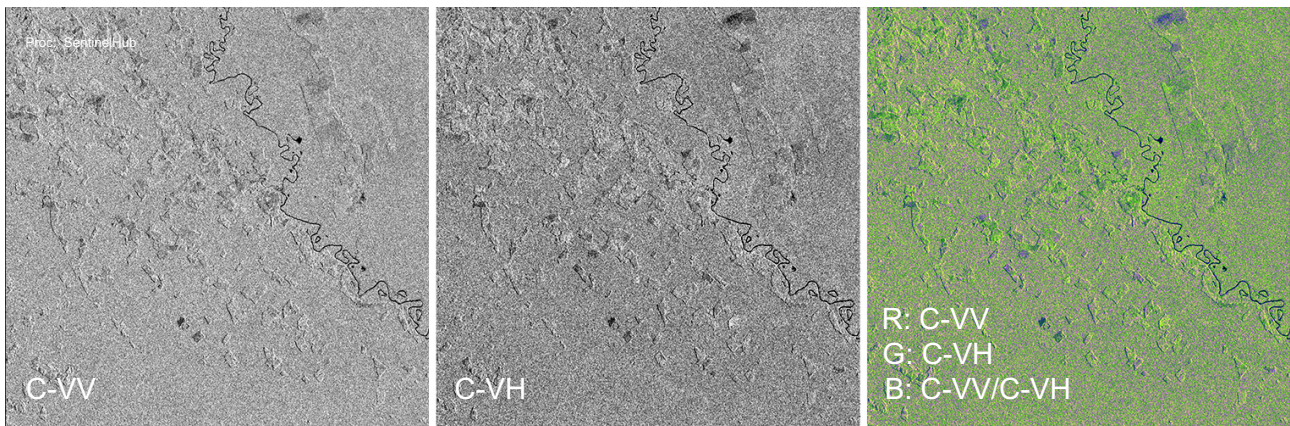
4.2.2 Forest removals and secondary growth (Colombia)

L-HH	L-HV	R: L-HH G: L-HV B: L-HH/L-HV |---- 10 km ----|
L-HH: -10.9 (+/- 3.5) dB	L-HV: -18.5 (+/- 4.1) dB	Observation date: 30-SEP-2017
C-VV	C-VH	R: C-VV G: C-VH B: C-VV/C-VH
C-VV: -8.4 (+/- 1.7) dB	C-VH: -13.1 (+/- 1.4) dB	Observation date: 30-SEP-2017

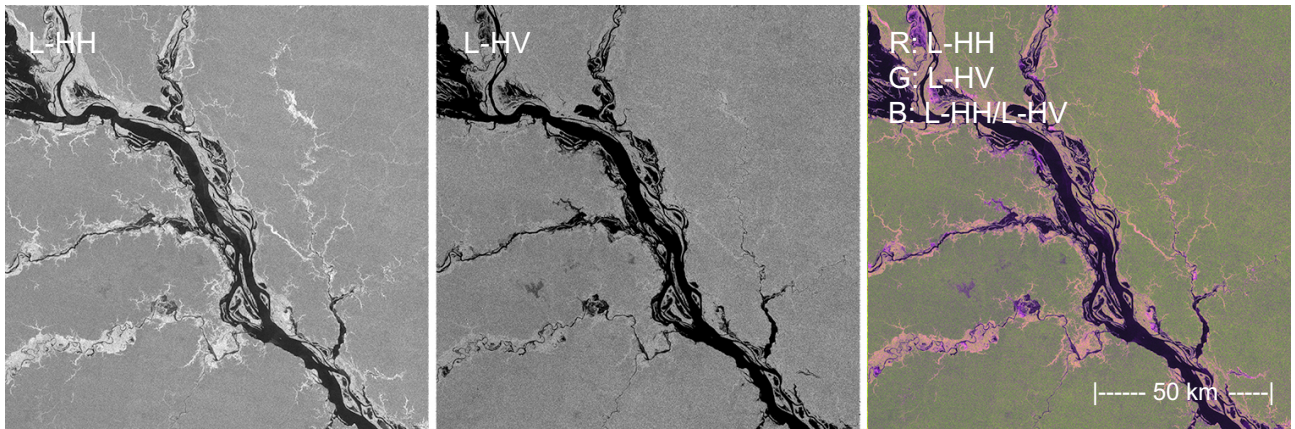Location: Caqueta, Colombia (N0.95º, W74.35º). Tropical forest conversion to mix of secondary growth and other land uses.

L-band:

In areas with deforestation and secondary forest growth, above-ground biomass levels (up to ~100 t/ha) are in the optimal range of sensitivity for L-band. The long wavelength provides for clear distinction between clear cut areas and different growth stages, with the HV channel having improved sensitivity to bare soil areas (very low backscatter) and displaying a wider radiometric dynamic range than the HH channel.

C-band:

Since the structure of leaves and small twigs in the top canopy of mature forest can resemble that of secondary growth vegetation, both provide similar backscatter responses at C-band. Rough soil conditions and remnant debris after deforestation can also produce a strong backscatter that, despite the lower above-ground biomass levels, can hamper distinction between different forest growth stages at C-band.
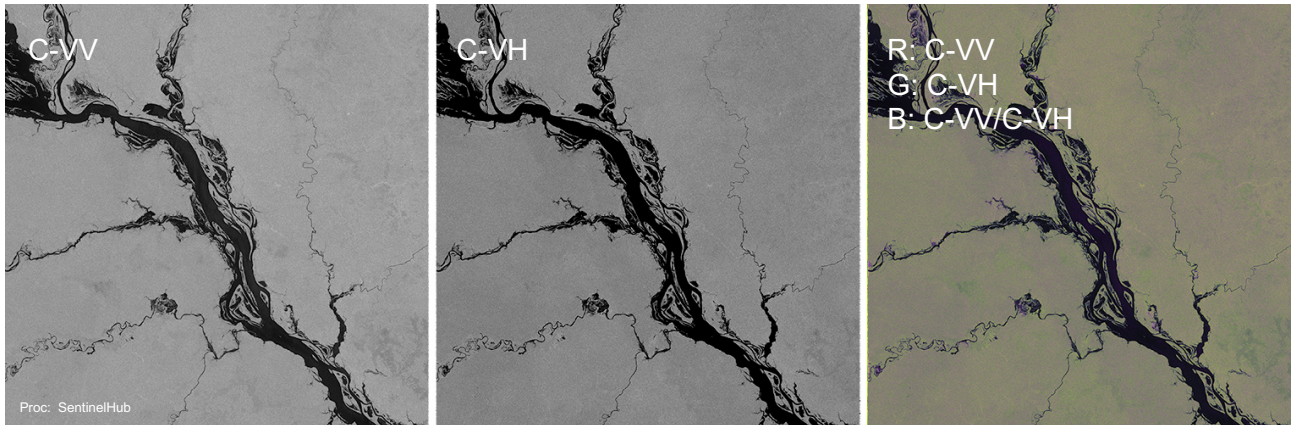
4.2.3 Forested wetlands (Brazil)

| L-HH: -2.9 (+/- 1.7) dB | L-HV: -12.7 (+/- 2.4) dB | Observation date: 18-AUG-2022 |

| C-VV: -6.5 (+/- 1.1) dB | C-VH: -12.3 (+/- 1.2) dB | Observation date: 18-AUG-2022 |

Location: Rio Negro, Central Amazon Basin, Brazil (S1.65°, W61.50°). Seasonally inundated floodplain forest (bright areas in L-HH).
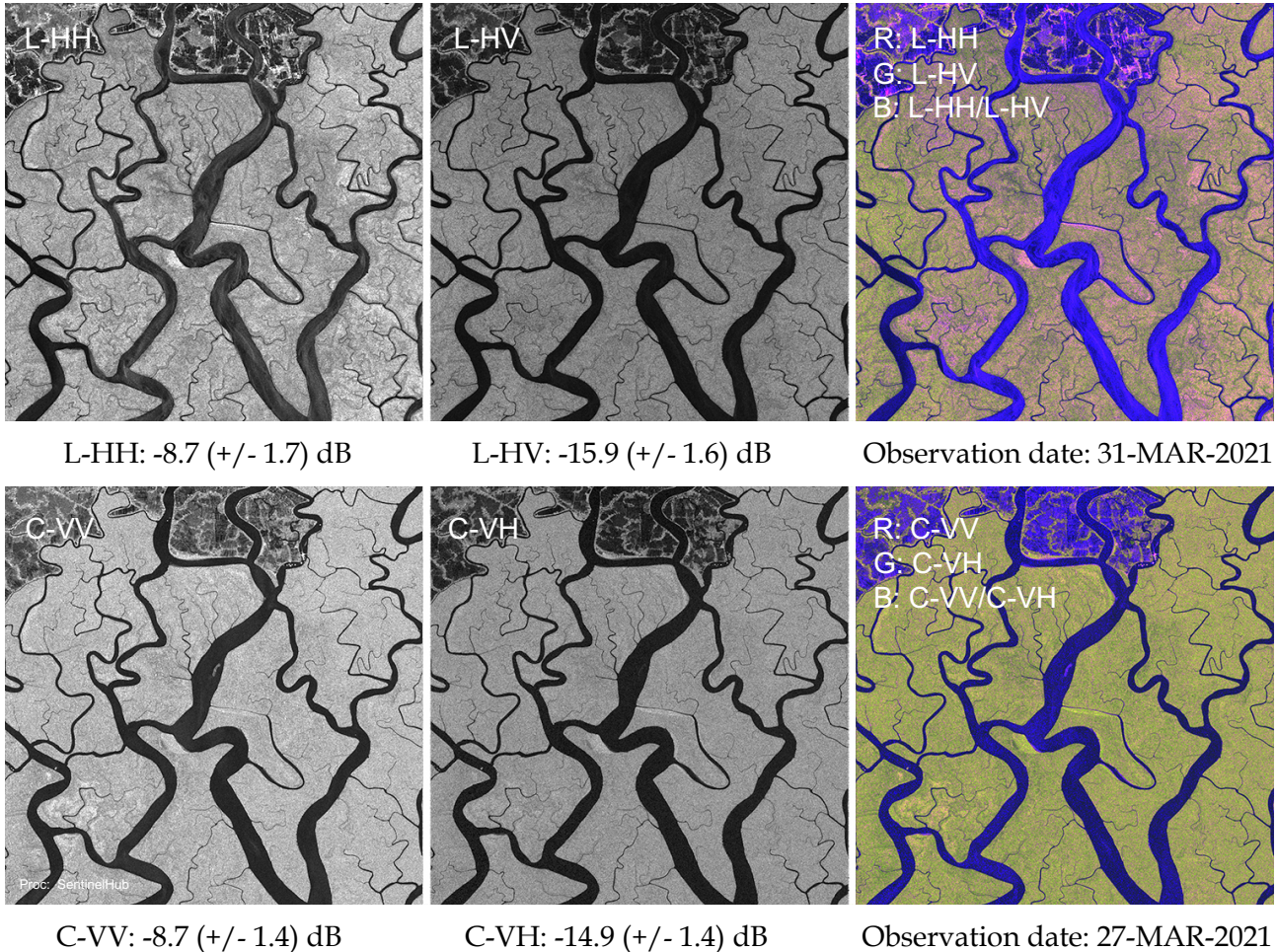
L-band:

In seasonally inundated floodplain forest, water floods parts of the forest floor during when river levels are high. With the L-band signal penetrating the canopy, the vertical stems and horizontal water surface give rise to a strong double-bounce reflection which produces an extremely high HH backscatter response. Flooded forest therefore appear very bright in HH polarisation. At HV polarisation on the other hand, which is dominated by volume backscatter only, the flooding extent is not visible and backscatter levels are similar to that of the surrounding non-flooded (dryland) forest.

C-band:

The density of the floodplain forest canopy does not change significantly between seasons, and the C-band backscatter therefore remains confined to the upper levels of the canopy regardless of any flooding below. C-band backscatter for inundated forest at both VV and VH polarisations are therefore not distinct from other forest types. In areas with sparser vegetation however, where the C-band signal can reach the water surface through gaps in the canopy, specular double-bounce reflection can be observed at VV polarisation also at C-band (see C-VV figure, south of river).

4.2.4 Mangrove (Bangladesh)

L-HH: -8.7 (+/- 1.7) dB   L-HV: -15.9 (+/- 1.6) dB   Observation date: 31-MAR-2021

C-VV: -8.7 (+/- 1.4) dB   C-VH: -14.9 (+/- 1.4) dB   Observation date: 27-MAR-2021

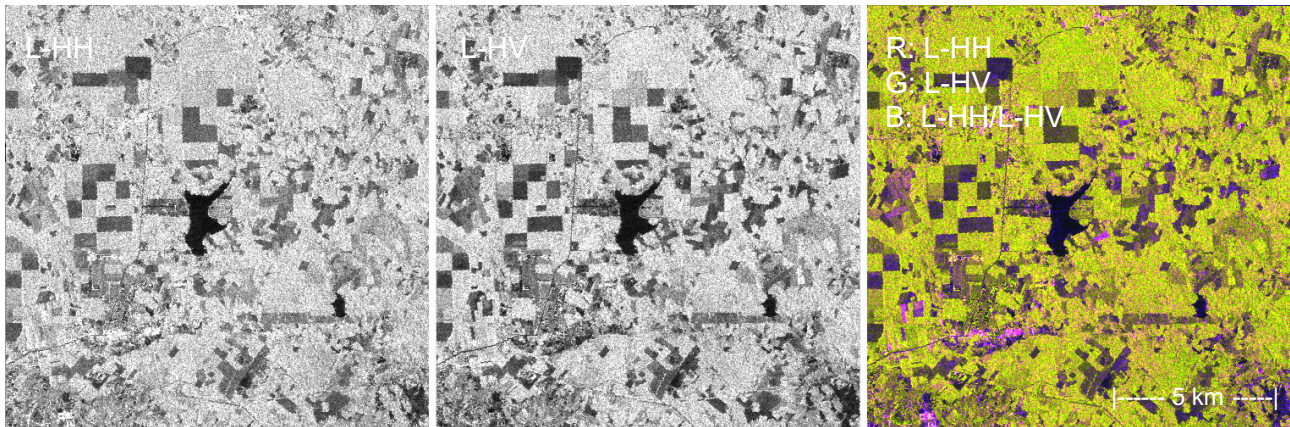Location: Sundarbans, Bangladesh (N22.1º, E89.3º). River delta with mangrove forest.

L-band:

In contrast to the inland floodplain forests example above, where vertical stems provide optimal conditions for specular double-bounce, the effect is typically not observed for dense mangrove forests, despite the presence of water under the canopy. The non-linear structure of the mangroves trees with their crooked branches and complex aerial root systems appear to impair double-bounce scattering. However, in areas with sparser mangroves, specular double-bounce does occur and results in increased HH backscatter (as can be observed in the right hand side of the L-HH image).

C-band:

Similar to the previous forest examples, C-band backscatter mainly occurs at the top of the canopy, with VV dominated by direct scattering. In areas with with patches of open water exposed, double-bounce scattering can occur (e.g. island in lower left part of C-VV image). At VH polarisation, the backscatter is low and caused by volume scattering at the top of the canopy.
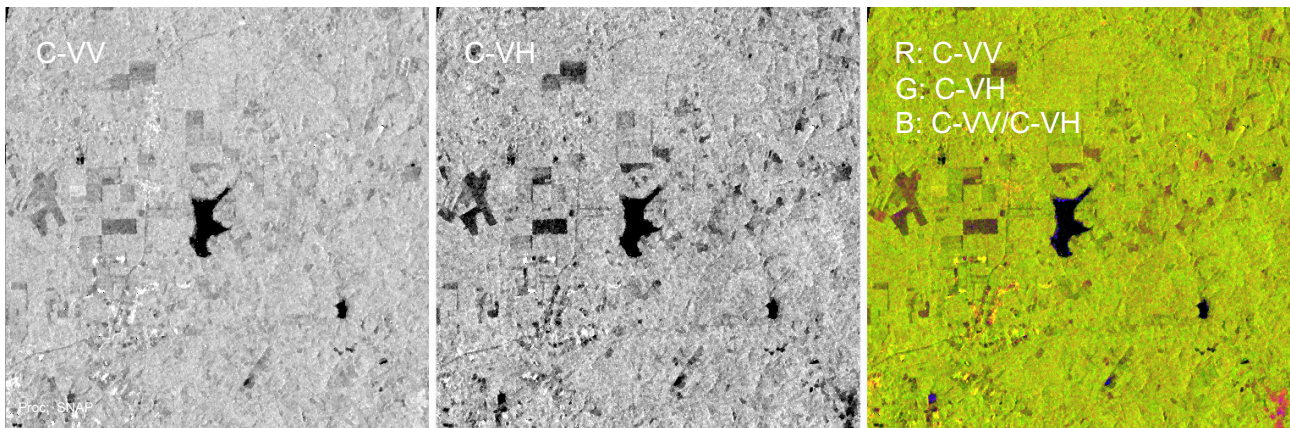
4.2.5 Forest plantations – Rubber (Vietnam)

L-HH: -4.8 (+/- 2.0) dB   L-HV: -10.6 (+/- 2.1) dB   Observation date: 8-SEP-2017

C-VV: -6.5 (+/- 1.2) dB   C-VH: -12.8 (+/- 1.1) dB   Observation date: 11-JUN-2017

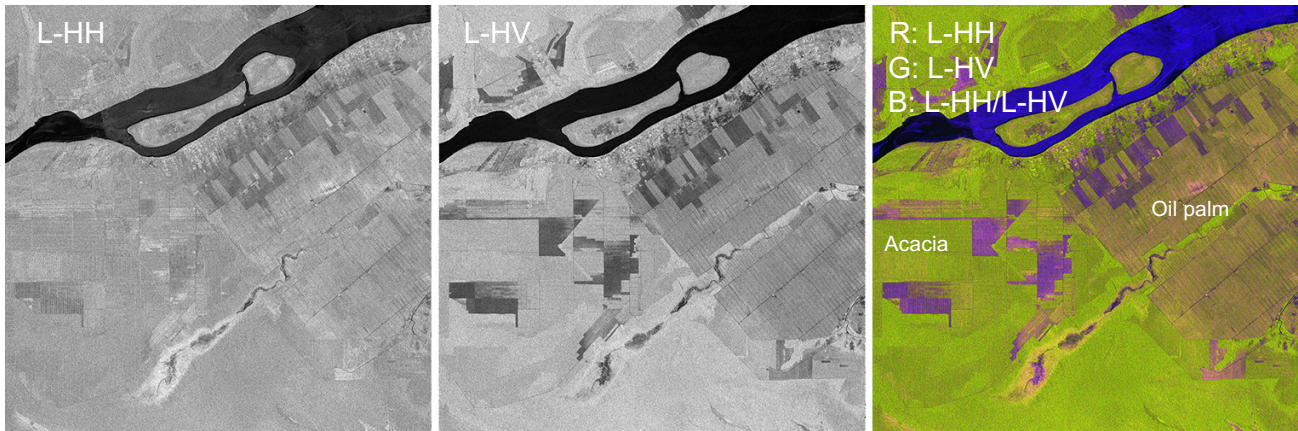Location: Binh Duong, Vietnam (N11.15º, E106.85º). Rubber plantations.

L-band:

Rubber plantations are dynamic landscapes characterised by a patchwork of forest stands at different ages that are cleared and replanted at 15~25 year intervals. L-band backscatter is correlated with the growth of young stands up to approximately 100 t/ha. Both HH and HV polarisations are sensitive to forest growth, with the HV polarisation channel providing a slightly larger dynamic range due to better distinction of cleared and bare soil areas than at HH.

C-band:

Rubber trees are deciduous with a leaf size of up to 13~15 cm, i.e. 2-3 times larger than the C-band wavelength (5.6 cm). The dominant backscatter mechanism is therefore direct canopy scattering similar to the other forest type examples above. Rubber stands however often feature a semi-open canopy with some gaps between the trees, which could allow for some limited penetration also at C-band and some limited sensitivity to rubber growth stage. No significant correlation was observed in the image analysed however. One potential reason for this could be the that the study area was located at the very far range of the Sentinel-1 image, and thus was observed at a too shallow incidence angle (~45º) for any openings in the canopy to be visible.

20

4.2.6 Forest plantations – Oil palm and Acacia (Indonesia)
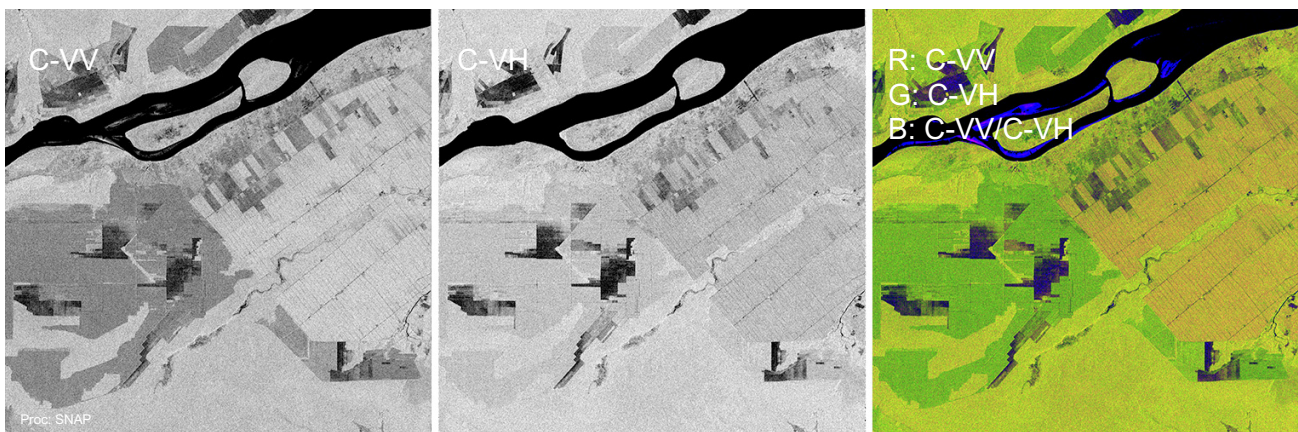

Oil palm: L-HH: -7.2 (+/-1.9) dB   L-HV: -14.6 (+/-1.9) dB   Observation date: 7-OCT-2017

Acacia: L-HH: -7.2 (+/-2.0) dB   L-HV: -12.3 (+/-1.8) dB

Oil palm: C-VV: -5.7 (+/-1.2) dB   C-VH: -13.3 (+/-1.1) dB   Observation date: 2-OCT-2017

Acacia: C-VV: -9.0 (+/-1.0) dB   C-VH: -13.0 (+/-1.0) dB

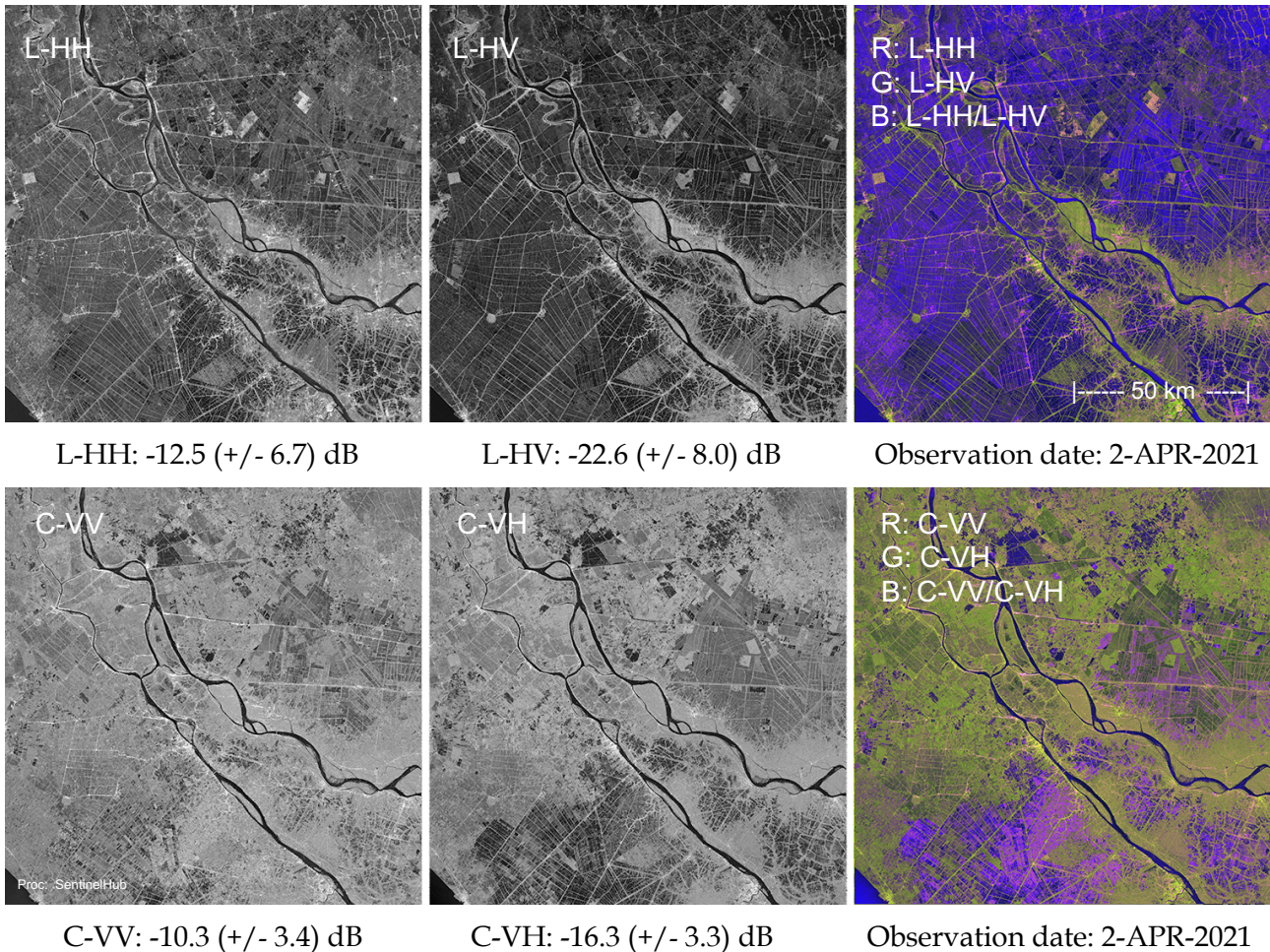Location: Riau, Indonesia (N0.15º, E102.95º). Oil palm and Acacia plantations.

L-band:

Oil palms have dense canopies made up of large palm fronds that effectively prevent any signal penetration even at L-band. L-band backscatter is therefore confined to interaction at the top of the canopy and correlates with crown growth rather than stem biomass. For *Acacia,* the signal is partly attenuated by the long (~20 cm) oblong leaves in the canopy, resulting in a slightly lower HH and HV backscatter than for natural forest. HV backscatter is correlated with Acacia growth stages.

C-band:

Oil palm backscatter mechanisms at C-band backscatter are similar to those for L-band, dominated by strong direct reflections on the top of the crowns. Like in L-band, oil palms have a reddish colour in C-band RGB composites due to dominant direct co-polarisation scattering. *Acacia* is easily distinguishable at C-band due to a weak response at VV and strong response at VH polarisation, resulting in a greenish appearance in the C-band RGB composite.

4.2.7 Agriculture – Irrigated rice (Vietnam)

L-HH: -12.5 (+/- 6.7) dB   L-HV: -22.6 (+/- 8.0) dB   Observation date: 2-APR-2021

C-VV: -10.3 (+/- 3.4) dB   C-VH: -16.3 (+/- 3.3) dB   Observation date: 2-APR-2021

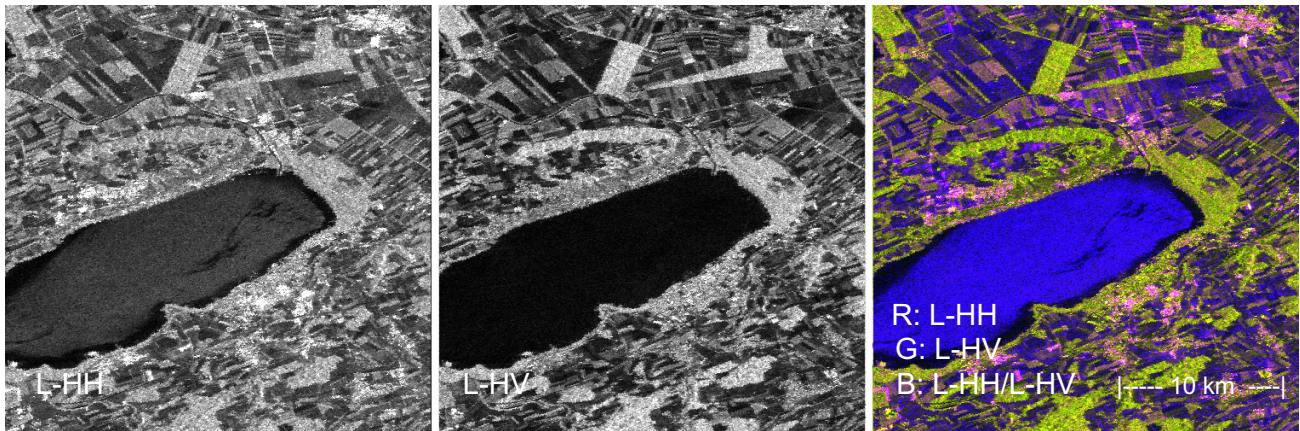Location: Mekong delta, Vietnam (N10.50°, E105.5°). Irrigated rice paddies.

L-band:

Irrigated rice growth is clearly visible in L-band SAR data. Reflections between the vertical rice plants and the water surface of the flooded fields can result in a strong HH double-bounce backscatter, which increases throughout the vegetation season from planting to harvest. The HV response is dominated by volume scattering in the plant canopy and thus sensitive to rice plant biomass. In the (top) figure above, acquired during planting and early growth stages, the image is still dominated by low HH backscatter, giving the RGB composite image a purple appearance.

C-band:

Dual polarisation C-band is perhaps perfectly apt for irrigated rice monitoring, where the VV and VH backscatter are dominated by specular double-bounce and volume scattering, respectively. The shorter C-band signal displays stronger sensitivity than L-band also to the early growth stages when the young rice plans are too small to be detected at L-band. This is illustrated in the bottom figure above, where the wide range of different colours in the C-band RGB image represent growth stage variations between the fields.
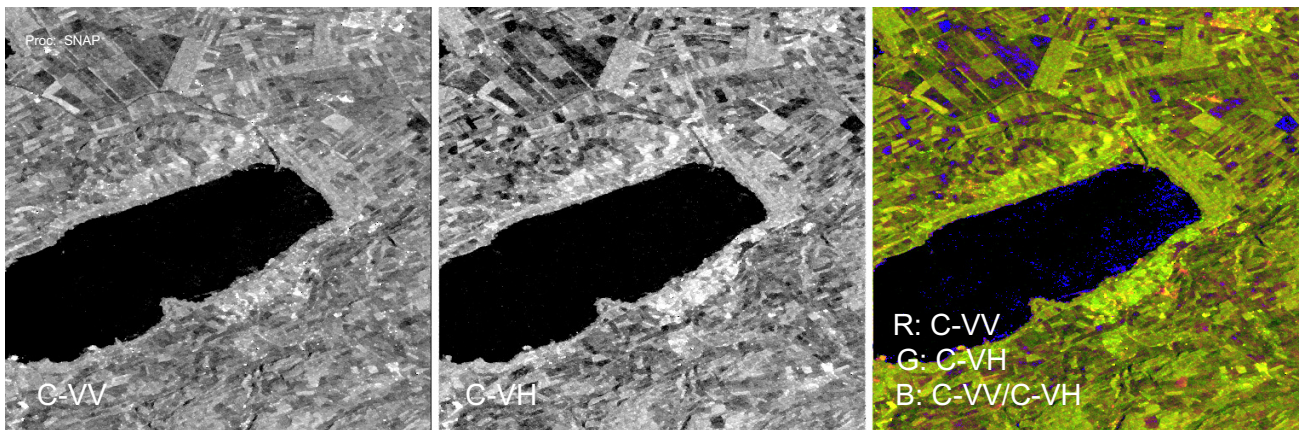
4.2.8 Agriculture (Switzerland)

L-HH: -11.7 (+/- 5.1) dB	L-HV: -20.5 (+/- 6.3) dB	Observation date: 16-SEP-2017
C-VV: -11.3 (+/- 2.3) dB	C-VH: -17.8 (+/- 2.6) dB	Observation date: 17-SEP-2017

Location: Murtensee/Freiburg, Switzerland (N46.95º, E7.10º). Mixed agriculture area with forest patches.
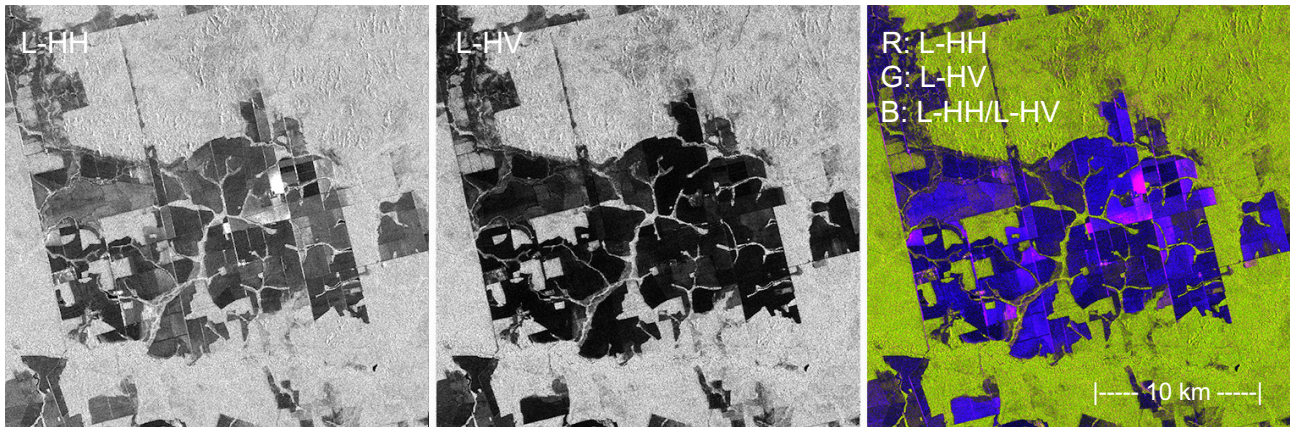
L-band:

In contrast to the paddy fields in the previous example, non-flooded (dryland) agricultural crops are largely transparent at the L-band wavelength, and signified by very low HV backscatter. The higher backscatter observed in the HH channel is likely not caused by the crop vegetation, but by direct scattering on ploughed fields and rough open soil. Agricultural areas typically have a purple appearance in the L-band RGB composite. The agricultural landscape can also be identified by geometrical patterns and textural features in the image, such as fields, roads and waterways. Isolated stands of forest appear green due to higher HV backscatter.

C-band:

Dryland crops are clearly visible in C-band data, with strong correlation between VH polarisation backscatter and plant growth, as illustrated by the dominant green colours in the C-band RGB composite above. A dense crop canopy can result in a backscatter response similar to that of forest. C-band VV backscatter is also correlated with plant growth but can cause confusion for newly planted or harvested fields where soil roughness is likely to be the major cause for scattering
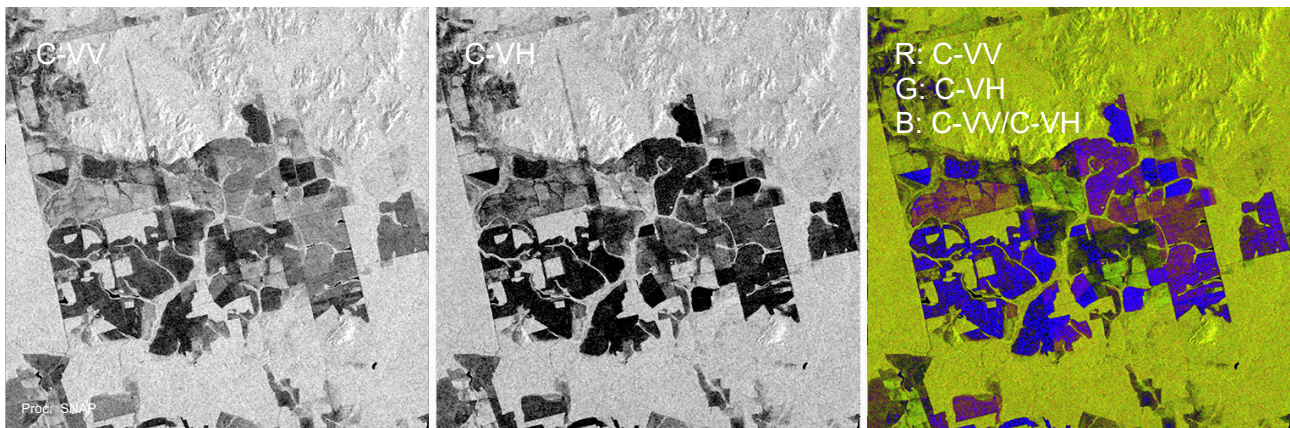
4.2.9 Rangelands and pastures (Brazil)

| L-HH: -14.0 (+/- 7.2) dB | L-HV: -24.4 (+/- 14.1) dB | Observation date: 3-FEB-2017 |
| C-VV: -12.0 (+/- 2.3) dB | C-VH: -19.4 (+/- 2.7) dB | Observation date: 31-AUG-2017 |

Location: Mato Grosso, Brazil (S10.05°, W51.85°). Rangelands and pastures.
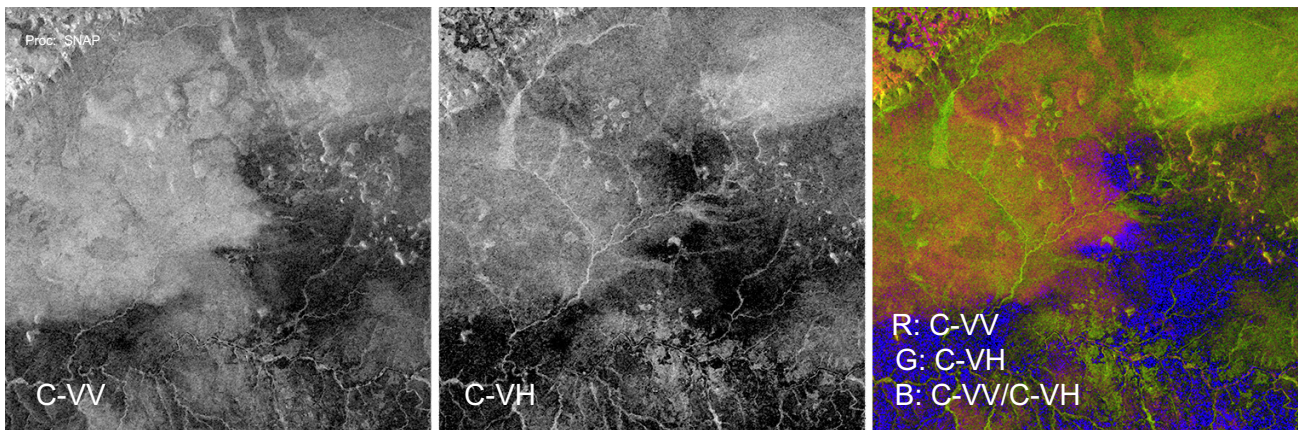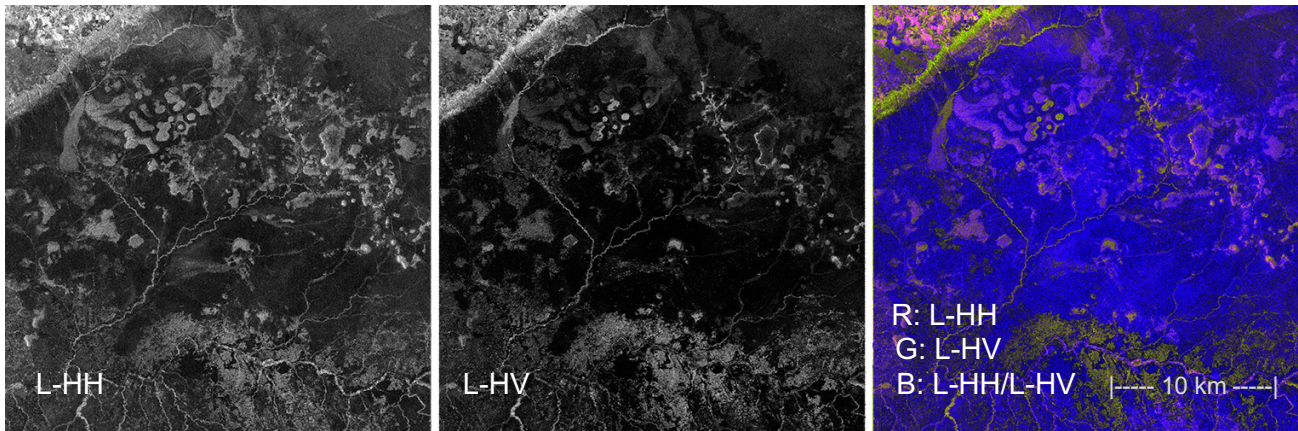
L-band:

The large cattle ranges in Mato Grosso are dominated by pasture grasslands. Due to the absence of vegetation at the size of the L-band wavelength (23.5 cm) and larger, backscatter is very low at both HH and HV polarisation. Pasture land is practically indistinguishable from bare soil, which both don a bluish colour in the L-band RGB composite image.

C-band:

At C-band on the other hand, pastures with different vegetation (structure, growth stages) produce a range of different responses at both VV and VH polarisation, as manifested by the variety of colours in the C-band RGB composite. Non-vegetated fields with smooth surfaces that were not distinguishable at L-band from grassy fields can be identified by their low response at both VV and VH and blue colour in the RGB image. The bright areas surrounding the fields in the image are remaining tropical forest yet to be cleared.

4.2.10 Savannah (Tanzania/Kenya)

L-HH

L-HH: -15.8 (+/- 5.2) dB

L-HV

L-HV: -24.9 (+/- 8.2) dB

R: L-HH
G: L-HV
B: L-HH/L-HV |---- 10 km ----|

Observation date: 10-FEB-2017

Proc: SNAP

C-VV

C-VV: -10.6 (+/- 2.2) dB

C-VH

C-VH: -17.5 (+/- 2.0) dB

R: C-VV
G: C-VH
B: C-VV/C-VH

Observation date: 24-FEB-2017

Location: Serengeti, Tanzania & Masai Mara, Kenya (S1.45°, E34.84°). Savannah (rainy season).
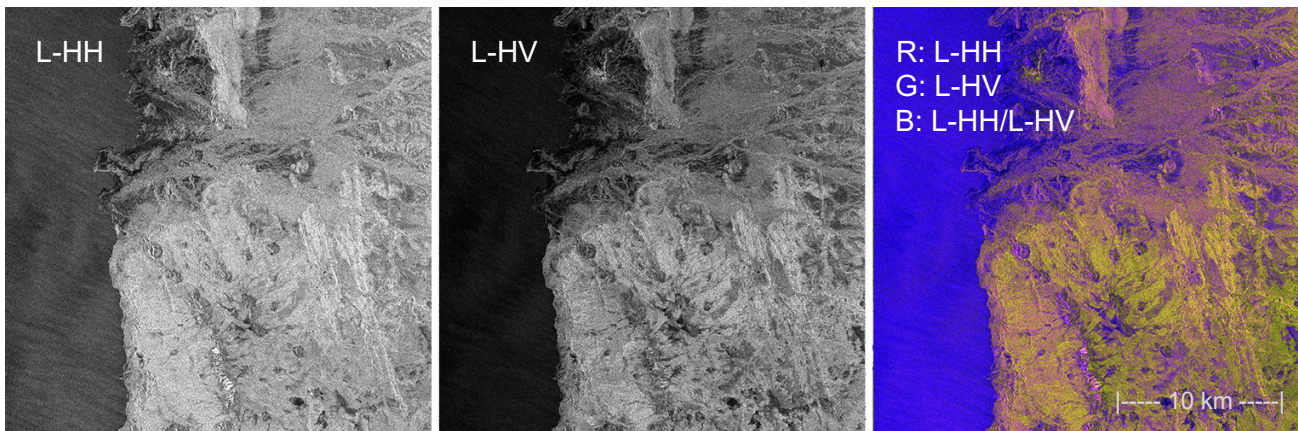
L-band:

The vast savannah landscapes of East Africa are dominated by large expanses of grasslands dotted by clumps of trees and bush vegetation. The grassy savannah vegetation is transparent at L-band and results in very low return at both HH and HV polarisation. Due to the lack of volume scattering the HV backscatter is close to the noise floor of the radar. The slightly brighter features visible are caused by riparian vegetation along the river channels, and likely by clumps of bushes and trees.

C-band:

As mentioned previously for the Brazilian rangelands, the shorter C-band wavelength is highly sensitive to grasses and low vegetation, which produce a strong response at both VV and VH polarisation. The different colours visible in the C-band RGB composite above indicate variations in the savannah vegetation structure that are not visible at the longer L-band wavelength. The blue region in the central part of the image, which displays low backscatter at both co- and cross-polarisation, is likely a smooth bare soil area. As February represents rainy season in the area, high moisture content of the soil likely contributes to the low backscatter from the bare soil areas.
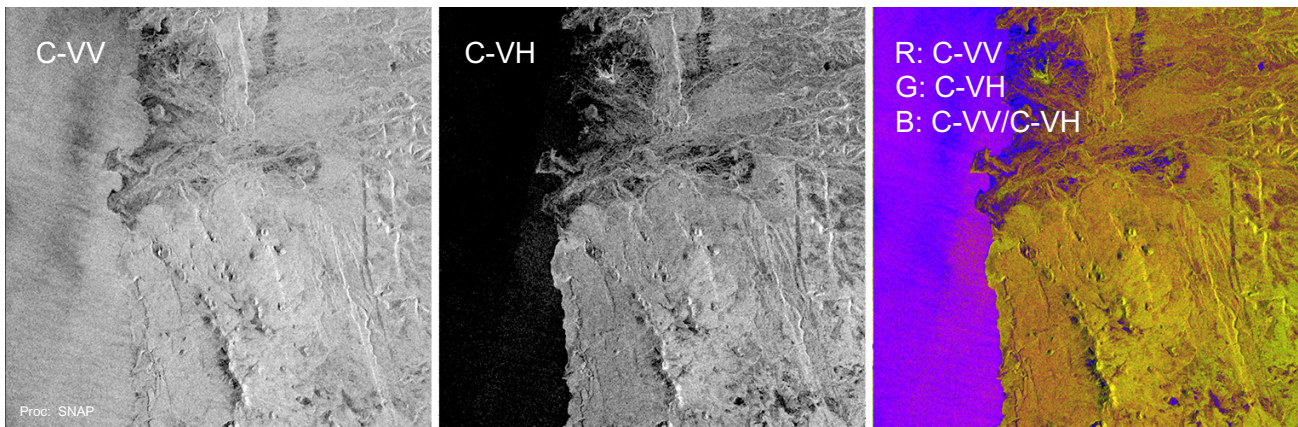
25

4.2.11 Arid terrain and rock outcrops (Kenya)

L-HH	L-HV	R: L-HH G: L-HV B: L-HH/L-HV |---- 10 km ----|
L-HH: -6.9 (+/- 2.5) dB	L-HV: -15.1 (+/- 2.9) dB	Observation date: : 1-OCT-2017
C-VV Proc: SNAP	C-VH	R: C-VV G: C-VH B: C-VV/C-VH
C-VV: -8.3 (+/- 2.0) dB	C-VH: -18.4 (+/- 3.1) dB	Observation date: 10-OCT-2017

Location: Marsabit, Kenya (N2.60º, E36.80º). Arid landscape with exposed bedrock.
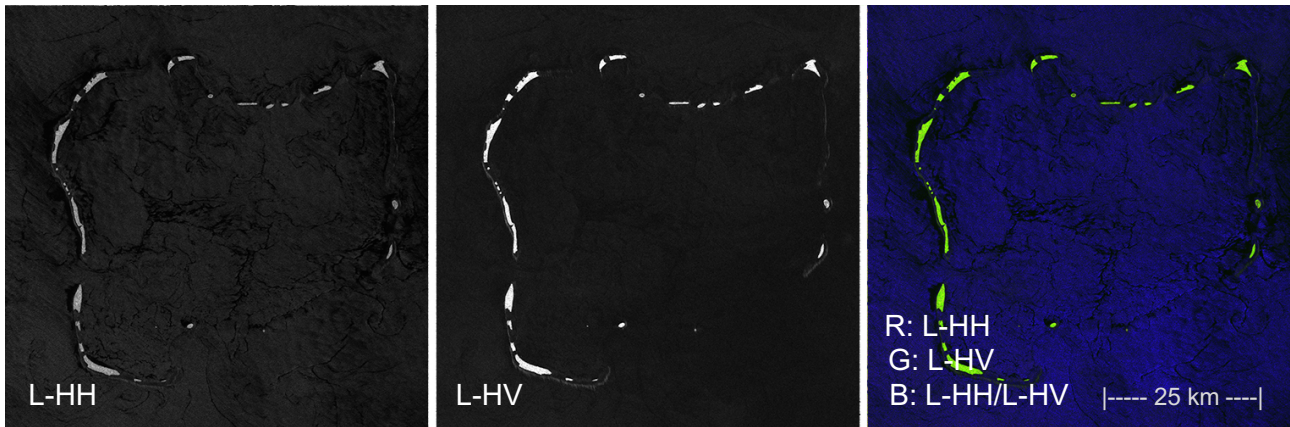
L-band:

Rough and uneven terrain around Lake Turkana results in strong L-band surface reflections and high HH backscatter. The moderate backscatter also at HV polarisation indicates multiple scattering effects that possibly could be caused by the presence of large rocks.

C-band:

C-band backscatter mechanisms for arid rocky terrain resembles that of L-band, with high reflections at VV polarisation and moderate at VH polarisation. The uniform HV response indicates an absence of even low vegetation, and supports the theory posed for L-band above that it could be due to rocks on the ground.
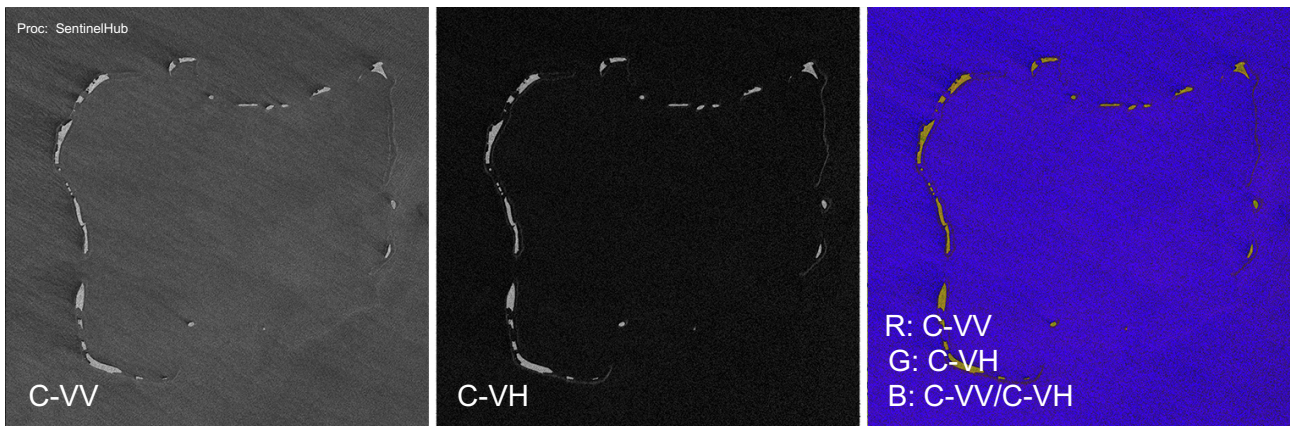
4.2.12 Open water (Mauritius)

L-HH: -27.6 (+/- 4.0) dB   L-HV: -38.9 (+/- 1.4) dB   Observation date: 26-JUN-2021

C-VV: -16.6 (+/- 1.6) dB   C-VH: -35.1 (+/- 5.8) dB   Observation date: 15-SEP-2021

Location: Chagos archipelago, Mauritius (S5.35º, E1.85º). Open water.
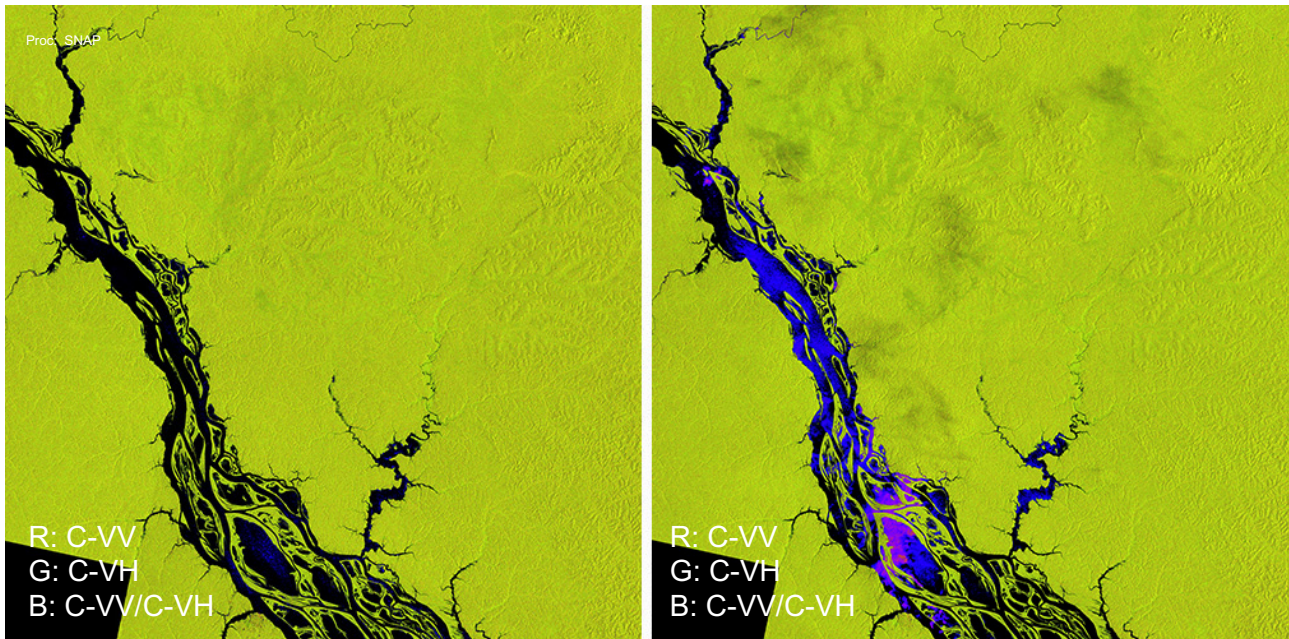
L-band:

Open water surfaces appear dark in L-band HV imagery and result in backscatter levels very close to the sensor noise floor. At HH polarisation, a smooth water surface similarly results in no scattering back to the sensor, while waves on the water surface can result in a small but distinct increase in backscatter. Faint wind patterns are visible in the L-HH image.

C-band:

C-band VV backscatter is highly sensitive to water surface roughness and can vary considerably depending on the occurrence of wind or rain during the acquisition. A prevailing wind towards northwest can be seen in the C-VV image, with somewhat lower backscatter on the tail wind side of the islands. As backscatter from open water is heavily dominated by direct surface scattering, C-band VH-backscatter typically remains very low, close to the noise floor, in most cases. During strong storm events however, also the VH backscatter can increase several dB due to multiple scattering effects on the rough water.

Note: the L- and C-band images were not acquired simultaneously and do not show the same surface conditions.

4.2.13 Signal attenuation (Brazil)

R: C-VV
G: C-VH
B: C-VV/C-VH

R: C-VV
G: C-VH
B: C-VV/C-VH

Sentinel-1 (C-band) 28-MAY-2017   Sentinel-1 (C-band) 04-MAY-2017 (heavy rain)

Location: Central Amazon basin, Brazil (S2.25°, W60.75°).

Microwave signals can under certain conditions be severely affected by atmospheric conditions and local weather events. In the example above, the left image shows a section of the Negro River floodplain acquired by Sentinel-1 during (assumed) "normal" weather conditions, while the right image shows the same area acquired by the same sensor a few weeks earlier during a heavy rain storm. The darker "cloud-like" features visible in the central part of the right image are caused by attenuation of the C-band radar signal by the dense rain clouds. Wave effects caused by the heavy rain and/or strong wind are also visible on the water surface (blue/purple in the RGB image).

The degree of signal attenuation by heavy rain is inversely proportional to the radar wavelength, with C-band (~5.6 cm) moderately affected and X-band (~3.1 cm) more severely so. X-band signals can under certain circumstances be completely absorbed, leaving no-data voids in the images. At the longer L-band wavelength (~23.5 cm) signal attenuation is generally not observed, although heavy rain can result in *increased* (HH) backscatter over forested areas due to the increased moisture content in the forest canopy.

While these kind of artefacts may be relatively easy to detect over homogeneous forest areas such as the example above, they can of course occur over all kinds of land cover and can bias and distort applications and results. Although the phenomenon cannot be avoided or corrected for, the impact can be mitigated by using data time-series (when applicable) to help identify and discard affected scenes.

5   Resources and references

ALOS-2 PALSAR-2 25m global mosaics (Japan Aerospace Exploration Agency)

JAXA 25m global mosaic download homepage:
https://www.eorc.jaxa.jp/ALOS/en/palsar_fnf/fnf_index.htm

Global mosaic format description:
https://www.eorc.jaxa.jp/ALOS/en/dataset/pdf/DatasetDescription_PALSAR2_FNF_v200a.pdf

Global mosaic reference paper:

Shimada, M. Ortho-Rectification and Slope Correction of SAR Data Using DEM and Its Accuracy Evaluation. IEEE Journal of Selected Topics in Applied Earth Observations and Remote Sensing. Dec. 2010, vol. 3, no. 4, pp 657 – 671.

Sentinel-1 (European Space Agency)

Copernicus Open Access Hub
https://scihub.copernicus.eu

Sentinel-1 SAR User Guide
https://earth.esa.int/web/sentinel/user-guides/sentinel-1-sar

Sentinel-1 SAR Technical Guide
https://earth.esa.int/web/sentinel/technical-guides/sentinel-1-sar

CEOS

CEOS Data & Tools
http://ceos.org/data-tools/

CEOS Analysis Ready Data
http://ceos.org/ard/

Others

Alaska Satellite Facility – Sentinel-1 data hub
https://www.asf.alaska.edu/sentinel

Document reference:

Rosenqvist A., Killough B., Dyke G. & Borges D., *A Layman's Interpretation Guide
to L-band and C-band Synthetic Aperture Radar data, v. 3.0* (May 2023).
Report for the Committee on Earth Observation Satellites.
http://ceos.org/ard/files/Laymans_SAR_Interpretation_Guide_3.0.pdf

Comments and suggestions welcome to
ake.rosenqvist@soloEO.com